RSC Advances

ROYAL SOCIETY OF CHEMISTRY

www.rsc.org/advances

Study of formaldehyde adsorption on silicene with point defects by DFT method

Xiao Wang,[*a] Huazhong Liu[b] and Shan-Tung Tu[c]

[a] School of Science, East China University of Science and Technology, Shanghai 200237, China.

[b] Department of Equipment Economics Management, PLA Military Economics Academy, Wuhan 430035, China

[c] Key Laboratory of Pressure Systems and Safety, Ministry of Education, East China University of Science and Technology, Shanghai 200237, China

* Corresponding author: *E-mail:* laricswang@gmail.com

Abstract

To explore the chemical activity and the sorption capacity of silicene with point defects for formaldehyde (HCHO), the interactions between HCHO and silicene are investigated using density functional theory (DFT). As compared to the weak adsorption on perfect silicene, HCHO molecule tends to be chemisorbed to the Si-Si bond of defective silicene with appreciable adsorption energy. However, the electronic conductance changes obviously by the adsorption of HCHO molecule on silicene containing Stone-Wales (SW) defects, while silicene with double vacancy still shows indirect semiconductor characteristic after HCHO adsorption. Moreover, the adsorption energy of HCHO on SW defected silicene (SW-Si) exhibits a continuously enhancement under the tensile strain up to 10%, suggesting the chemical reactivity of SW-Si sheet increases by applying external strain.

1. Introduction

High mechanical strength, chemical stability, and unique electronic properties have made graphene a material of interest in diverse fields ranging from biotechnology to electronics in recent years.[1-3] As the counterpart of graphene, monolayer silicon called silicene has also attracted much attention due to its exotic electronic properties similar to graphene and promising applications in Si nanoelectronics.[4] Theoretical calculations have revealed that in a silicene structure a hexagonal mesh of silicon atoms is bulked and the electronic structure of silicene is equivalent to graphene with linear electronic dispersion resembling that of relativistic Dirac fermions.[5-8] Experimentally, many groups have reported the successful preparation of silicene on Ag (110),[9,10] Ag(111)[11,12] and Ir (111).[13] The structural parameters and electronic structures of these sheets are in good agreement with the theoretical predictions. In addition, the Si atoms in silicene prefer to form a sp^2-/sp^3-hybridization which is essentially different from the sp^2 hybridization of graphene. Thus silicene possesses much higher chemical activity towards foreign adsorbates than graphene, such as NO and NH_3.[14]

Several studies have shown that graphene usually suffers various types of topological defects during its growth. The existence of defects, such as vacancies, Stone-Wales (SW) defect can induce magnetism, tailor the electronic properties and alter the chemical activity of graphene-based structures.[15-17] Most recently, Sahin et al. studied silicene with SW defects using first-principles calculation.[18] It was found that the energy barrier for the formation of SW defects in silicene is significantly lower

than in graphene and the buckled nature of silicene provide a large energy barrier for the healing of the SW defects. Existence of SW defect induces small gap of 0.02 eV and this value depends on the concentration of defects. Furthermore, the investigation of other kinds of defects, single and double vacancies (SVs and DVs) in silicene has shown that SV vacancy is unstable and two SVs are likely to coalesce into one DV to lower the energy.[19] Since SW defects and DV stably exist in silicene and affect their electronic characteristics, it is highly wondering that how the point defects influence their chemical activity. In addition, based on the previous studies,[20,21] mechanical strain can increase activity of carbon nanomaterials such as nanotubes and graphene. Hence, silicene requires further investigation.

Since silicene has a higher chemical activity, one of the potential applications of silicene is the field of sensor. For nanomaterials, the gas sensor is known to be actualized by monitoring the change in electronic conductance resulted from the adsorption molecules, which act as charge acceptors or donors.[22,23] Silicene used as gas sensor has been reported in Feng's work.[14] In their work, silicene interacts with NO and NH3, accompanying with charge transfer between molecules and silicene, the band gap is opened upon gas adsorption. On the other hand, Wu et al.[24] reported that reactivity of silicene can also be enhanced by applying extern strain. Thus, both defects and extern strain may affect the properties of silicene when it is used as sensor.

Formaldehyde (HCHO) is the most common and well-known indoor air pollutant because of its wide applications in many constructive and decorative materials. It can

cause headache, nausea, coryza, childhood asthma even lung cancer.[25,26] Therefore monitoring and controlling its exposure in both residential and industrial environments are very important. Many methods such as polarography, gas chromatography and fluorometry[27,28] have been developed to detect HCHO. However, these methods require complicated and expensive instruments and are not sensitive enough as they either have high detection limits, or require long sampling intervals. Thus, many studies have been reported to investigate the interaction of HCHO with nanomaterials, such as TiO_2,[29] CNT,[30] graphene,[31] and etc. However, little work has been done to study the interaction of HCHO and silicene.

Therefore, to understanding the influence of defect on the chemical activity of silicene and explore potential application of this promising material in detecting HCHO, in this paper, we present a detailed investigation on the adsorption behaviors of HCHO on perfect and two kinds of defected silicene (SW and DVs) based on density functional theory (DFT). It is found that different from HCHO binding with pristine silicene, the molecule can chemisorbs on both defective silicene sheets with high adsorption energy and obvious structural distortion. Especially, the electronic structures changed obviously by the adsorption of HCHO molecule in SW-defected silicene. Furthermore, the chemical activity of SW-defected silicene is enhanced by mechanical strain. The results may afford new insight into silicene applications in gas sensors and a simple approach to control the chemical activity of silicene.

2. Computational method

All the calculations were performed within the framework of unrestricted spin-polarized DFT, implemented in the Dmol3 code.[32-34] Structure optimizations and the corresponding total energy calculations of the most stable geometries are based on the generalized-gradient approximation (GGA) with the PerdewBurkeErnzerhof (PBE) correction,[35] and the all-electron calculations and a double numerical basis set plus polarization functional (DNP) are adopted.[33] The DNP basis set corresponds to a double-f quality basis set with a p-type polarization functions to hydrogen and d-type polarization functions added to heavier atoms, which is comparable with the Gaussian 6-31G (d, p) basis set and owns a better accuracy.

In this work, a 5 × 5 × 1 supercell with periodic boundary condition is used to model the infinite silicene sheet. The silicene sheet includes 50 atoms with lattice parameters of a = b = 19.33 Å. The vacuum space of 20 Å was set in the direction normal to the sheets to avoid the interactions between periodic images. The Brillouin zone is represented by the set of 10 × 10 × 1 k-points[36] for the geometry optimizations, and 15 × 15 × 1 k-points are used to obtain the density of states (DOS). The global orbital cutoff of 4.6 Å are set in the spin-unrestricted calculations for all systems, and the effect of periodic boundaries was negligible. All atoms are allowed to relax. Convergence in energy, force, and displacement is set at 10^{-6} Ha, 0.001 Ha/ Å, and 0.001 Å, respectively. The adsorption energy E_{ads} of HCHO molecule on pristine or defected silicene is defined as:

$$E_{ads} = E(\text{total}) - E(\text{sheet}) - E(\text{HCHO})$$

where E(total), E(sheet), and E(HCHO) are the total energies of relaxed silicene with an absorbed HCHO molecule, the isolated silicene sheet and the isolated HCHO molecule. Additionally, the stability of silicene is measured via its cohesive energy which is defined as the energy required for separating the crystal into isolated free atoms. The cohesive energy of a silicene structure is given by the formula

$$E_{coh} = (E_{tot/N}) - E_{Si} \quad (2)$$

where E_{tot} is the total energy of the system, N is the number of atoms in the supercell and E_{Si} is the total energy of an isolated silicon atom.

3. Results and discussion

3.1 Pristine and defective silicene with point defects

The computed lattice parameter of relaxed silicene is 3.866 Å and the Si−Si bond length is calculated to be 2.28 Å, consistent with previous studies,[37,38] as shown in Figure 1a. The larger Si−Si interatomic distance weakens the π−π overlaps and results in a low-buckled structure with h = 0.45 Å (Figure 1b). Silicene is also found to be a gapless semiconductor like graphene,[39,40] the bonding π and antibonding π* bands crossing only at K points in the hexagonal Brillouin zone (Figure 2).

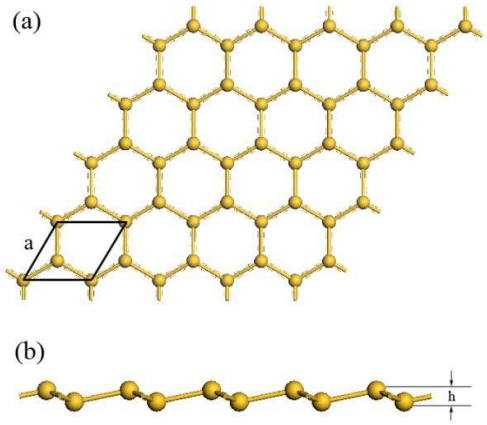

Figure 1. Optimized geometric strucutres of silicene from (a) top view and (b) side view. Silicon atoms are shown in yellow.

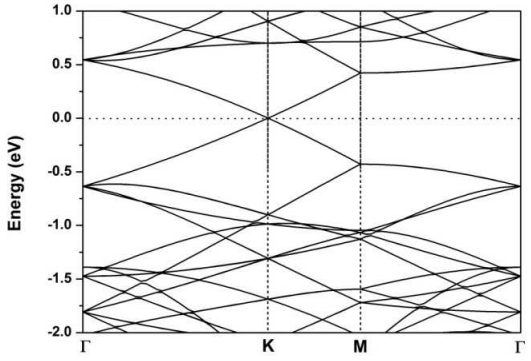

Figure 2. Band structure for a 5 × 5 supercell of perfect silicene. The Fermi level is set to 0 eV and presented in dots.

As shown in Figure 3, a SW defect in silicene can be created by the rotation of a silicon dimer by 90^{o} around the center of the Si-Si bond. After the formation of the SW defect, four neighboring hexagons of silicene are transformed into a pentagon and a heptagon pair. And through 90^{o} rotation of a dimer, the Si-Si bond becomes stronger than in perfect silicene and its length decreases from 2.28 to 2.189 Å. The cohesive

energies of silicene and SW-defected silicene are calculated to be −3.96 and −3.92 eV, respectively. The negative cohesive energies of both structures indicate their stability.

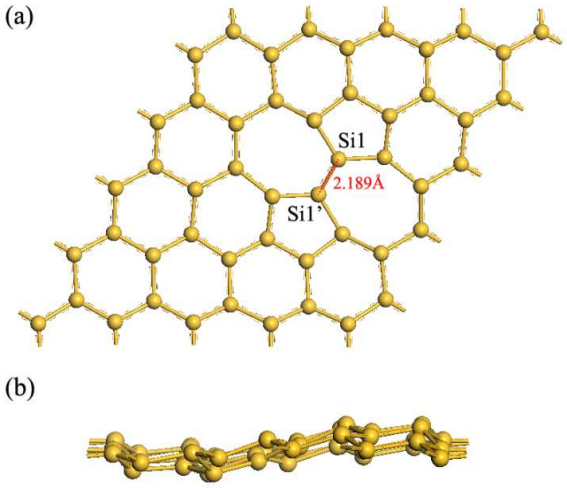

Figure 3. Optimized geometric strucutres of SW-defected silicene from (a) the top view and from (b) the side view.

The electronic band dispersion of SW-defected silicene (SW-Si) is presented in Figure 4. Since the formation of the SW defect breaks the six-fold symmetry of the silicene lattice, a small band gap of 0.028 eV opening occurs at the crossing point which agrees with the previous studies of silicene and graphene.[19,41] Noted that SW almost retaining the linear dispersion relationship near the Fermi level. Hence, a silicene with SW defects would open a small gap without harm to the high velocity carriers. Nevertheless, the SW defect induces a defect π state which is located about 0.3 eV above E_F. The defect π state is localized significantly at the Si1 and Si1' sites as seen in PDOS given in Figure 4(b). In addition, since there is no dangling bonds

introduced into the silicene lattice with the creation of a SW defect, all the atomic orbitals of Si atoms at the vicinity of the defect are paired and hence there is no defect-originated magnetism.

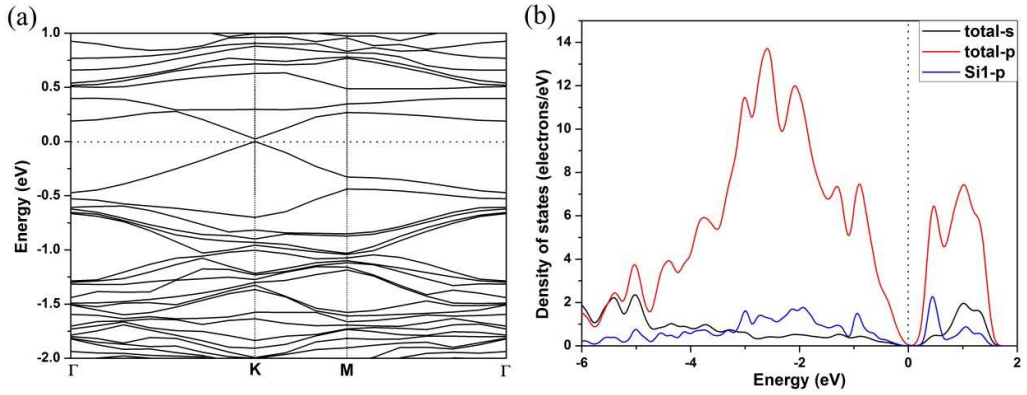

Figure 4. (a) Band structure of SW-Si and (b) PDOS for atoms around its defect region. The Fermi energy is set to zero eV and indicated in dots.

The case of divacancy is different from that of the SW defect. Here we could not observe obvious strengthened buckling behavior of atoms from the mean plane (see Figure 5) after optimization. The Si atoms around the vacancy constellation have moved inward forming two new bonds and reconstructed to be a 585 defect shown in Figure 6. The rearranged structure encloses a central octagon and two opposing pentagons. The Si-Si length with 2 unit cells is approximately reduced to 6.55 Å compared with the pristine Si-Si bond which has the length of about 7.73 Å. It is found that the length of the newly formed Si-Si bond stretches to 2.43 Å, and the other Si-Si bonds which form the octagon also stretch to share the tension induced by

the two missing atoms. The cohesive energy of this double vacancy defected silicene (DV-Si) is -3.90 eV, a littler higher compared with that of the SW defect.

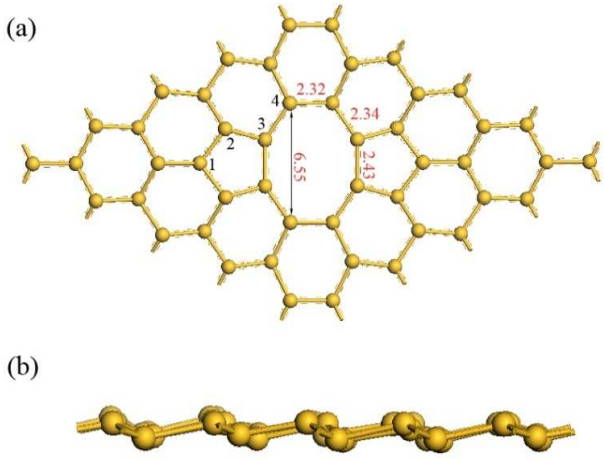

Figure 5. The top (a) and side (b) view of reconstructed atomic structures of silicene in the presence of 585 defects. The lengths of Si-Si bond are denoted by red numbers in Å.

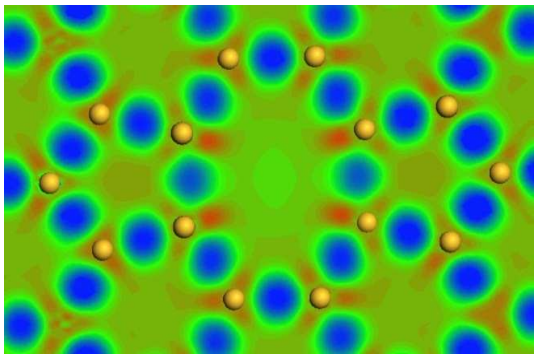

Figure 6. Deformation electron density of defective region of DV-Si.

The calculated band structure for this 585 DV-Si sheet is shown in Figure 7(a). The effect of the presence of the divacancy is apparent; it induces an dispersionless

π-character band state above the Fermi level and an indirect semiconductor with 0.14 eV band gap is obtained. From the PDOS for Si atoms around the defect region depicted in Figure 7(b), it is found that the main contributions of such band are dominated by the p_z states of Si1 atoms and Si3 and Si4 atoms next to vacancy site. In the previous studies on graphene with 585 defect,[42] it was predicted that a single impurity in sublattice A of graphene induces an impurity state mostly localized in sublattice B and vice versa due to the existence of two nonequivalent Dirac points. Because Si2 atoms belong to a sublattice different to the one of Si1 and Si3 atoms, there is almost no contribution from the former atoms to the defect states above the Fermi level.

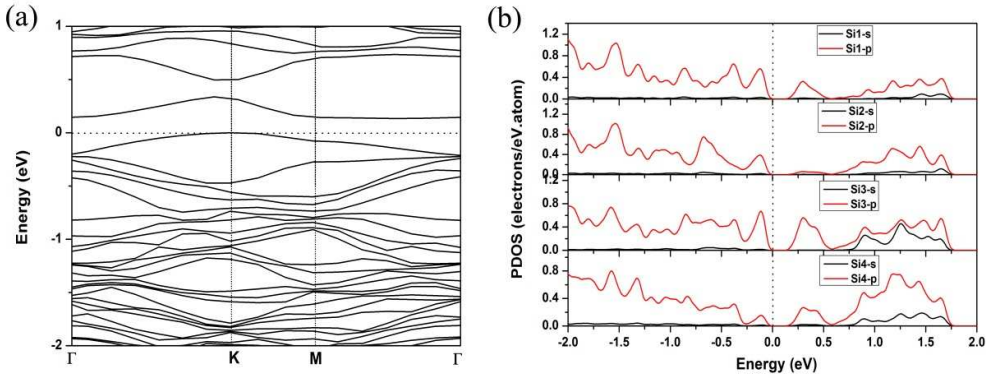

Figure 7. (a) Band structure of DV-Si and (b) its PDOS for atoms around its defect region. The Fermi energy is set to zero eV and indicated in dots.

3.2 Formaldehyde adsorption on pristine silicene

For the adsorption of HCHO on pristine silicene, different possible adsorption configurations are considered, including C, O or H atom of HCHO molecule closes to

the Si atom, respectively; C=O bond parallels the Si-Si bond and the HCHO molecule locates parallel to the hexagonal ring of silicene. All five stable configurations are observed after full optimization and the evaluated adsorption energies for these cases are given in Table 1. The obtained adsorption energies and the large interaction distances of all five configurations imply the weak physisorption of HCHO molecule on the pristine silicene sheet.

Table 1. The adsorption energy (E_{ads}) and the interaction distance between HCHO and the pristine silicene surface (d).

Model	E_{ads} (eV)	d (Å)
O closes to Si atom	-0.076	3.622
C closes to Si atom	-0.087	4.000
H closes to Si atom	-0.086	2.878
C=O bond parallels the Si-Si bond	-0.116	3.177
locates parallel to the hexagonal ring	-0.113	3.489

*For the models of O, C, H atoms close to Si atom, d means the distance between O, C, or H and the Si atom it closes to, respectively. When C=O bond parallels the Si-Si bond, d is the distance between O and Si atom.

3.3 Formaldehyde adsorption on SW defected silicene

Similarly, in order to find the most stable adsorption configuration, the HCHO molecule is initially placed at various positions above the SW-Si with different

orientations. The most stable configuration of the HCHO on SW-Si is shown in Figure 8, in which the C=O bond of HCHO attacks a Si-Si bond of the pentagon ring. The adsorption occurs through bonding O atom of the molecule with the Si atom of the SW defected silicene, and C atom with another Si atom, forming a four-membered ring. The E_{ads} is -1.389 eV, which is 1.173 eV lower than on the pristine silicene in the most stable configuration and also much lower than that of HCHO adsorption on SW defected graphene,[43] indicating that the interaction between HCHO and SW-Si is much stronger than with pure silicene or SW defected graphene. The interaction distances of C-Si and O-Si bonds are 1.963 and 1.704 Å, respectively. Moreover, HCHO adsorption induces a local structural deformation to both the HCHO molecule and the SW-Si sheet. The bond angle of H-C-H and two H-C-O of HCHO are significantly decreased from 116°, 122°, and 122° in free HCHO to 109.7°, 109.4°, and 110.1°, respectively, in the adsorbed form. The HCHO-adsorbed Si-Si bond is pulled outward from the silicene with the bond length increasing from 2.345 Å of SW-Si to 2.405 Å. Such strcutrural deformation is attributed to the change from sp^2-/sp^3- to sp^3 hybridization of Si atoms. The deformation of the system structure and the appreciable binding energy suggest that the interaction in this configuration belongs to chemisorption.

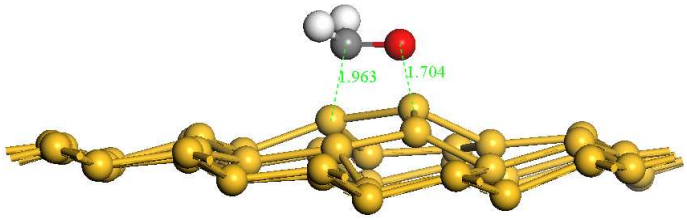

Figure 8. Optimized configuration of HCHO adsorbs on SW-Si

To investigate the charge transfer between SW-Si sheet and HCHO molecule, electron density difference Δρ for this configuration is evaluated; which illustrates how the charge density changes during the adsorption process and is defined as:

$$\Delta\rho = \rho_{total} - (\rho_{sheet} + \rho_{HCHO})$$

Where ρ_{total} , ρ_{sheet} and ρ_{HCHO} denote electron density for SW-Si sheet with adsorbed formaldehyde molecule, SW-Si sheet and HCHO molecule in the adsorbed form, respectively. Figure 9 shows the electronic density difference isosurfaces for this configuration; loss of electron is indicated in yellow, while electron enrichment is indicated in blue. It is clear that charge transfers from silicene to HCHO, in which some charges accumulate around the C and O atoms of HCHO, especially O atom. Therefore both reconstruction and charge transfer confirm the strong binding between HCHO and SW-Si sheet induced by adsorption. The above results are supported by data from the Mulliken charge analysis, where electrons around O atom increase from 0.312 to 0.557 e and that of C atom accumulates to 0.161 e. About 0.436 electrons are transferred from the silicene to the HCHO molecule, much larger than the charge transfer happened in the adsorption of NO or NH_3 on silicene.[14]

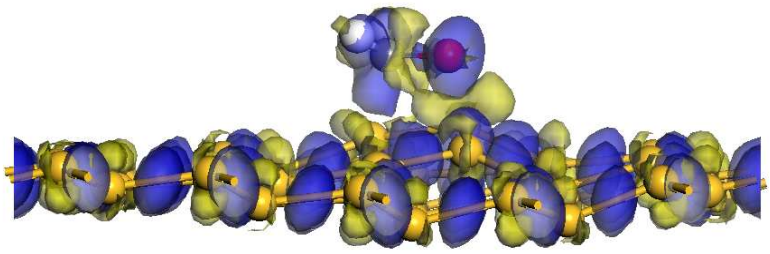

Figure 9. Charge density of HCHO adsorbed SW-Si sheet.

3.4 Formaldehyde adsorption on DV defected silicene

To investigate the effect of divacancy defect on HCHO adsorption, except those configurations with binding energies comparable to that of pristine silicene, there are two stable configurations exist (panel 1 and 2) after the geometry optimization shown in Figure 10. In both configurations, similar to HCHO adsorption on SW-Si, C=O bond of molecule interacts with the Si-Si bond of either in the pentagon ring or the octatomic ring. The adsorption of HCHO molecule pulls the adsorbed Si-Si bond out slightly from the silicene and induces a local structural deformation to the HCHO molecule. For example, in panel 2, the HCHO-adsorbed Si-Si bond is pulled outward from the silicene and the interaction distances of C-Si and O-Si are 1.950 and 1.708 Å, respectively. The adsorption energy of HCHO molecule on divacancy silicene are -1.577 and -1.644 eV, respectively, in contrast to the values using pristine silicene substrates, showing that the introduction of vacancy enhanced the interaction between the silicene and HCHO molecule significantly. Charge transfer between the HCHO molecule and the divacancy silicene substrate is also calculated by Mulliken population analysis. The results suggested that the HCHO molecule behaved as an

accepter grabbing charge from silicene, which is the same with HCHO adsorption on SW-Si sheet. The charge of panel 2 is 0.431 e, a littler higher than that of panel 1, and it agrees with its largest adsorption energy. The charge transfer analysis again indicated that the defect affected the adsorption process of HCHO molecule.

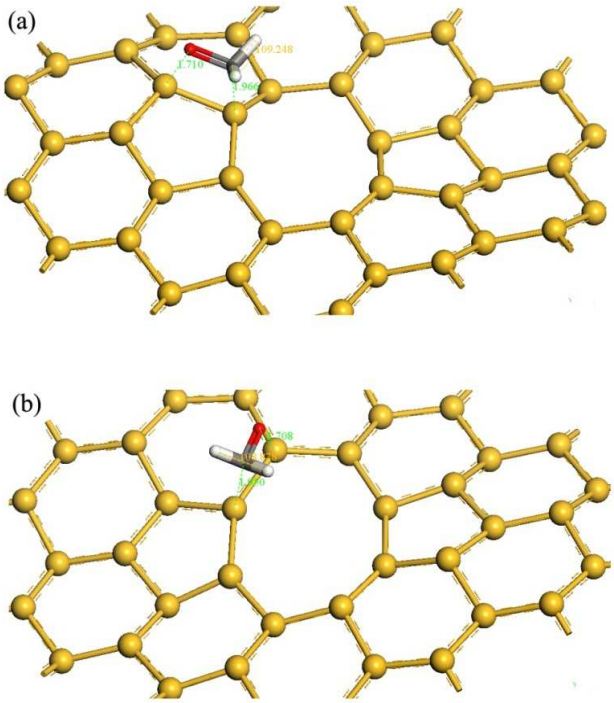

Figure 10. Optimized stable configurations of HCHO adsorbs on DV-Si sheet. (a), panel 1 and (b) panel (2).

3.5 Electronic structures

For detecting a molecule by a given sheet, one of the properties of the sheet (such as electrical conductivity) should be changed by the chemisorption of molecule. The obtained results have shown that HCHO molecule is just chemisorbed on SW-Si

or DV-Si sheets. Thus, to check the sensitivity of the sheets to the adsorption of HCHO molecule, the electronic structures of the considered configurations are investigated through analyzing their band structures; spin polarized DOS and partial density of states (PDOS) spectra.

In the case of DV-Si sheet, the presence of the divacancy induces an almost dispersionless band state above the Fermi level and the system becomes an indirect semiconductor. It is clear in Figure 11 that upon the chemisorption of HCHO molecule on DV-Si sheet, no distinct change occurs in its electronic properties, hence this sheet is not suitable for detecting HCHO molecule.

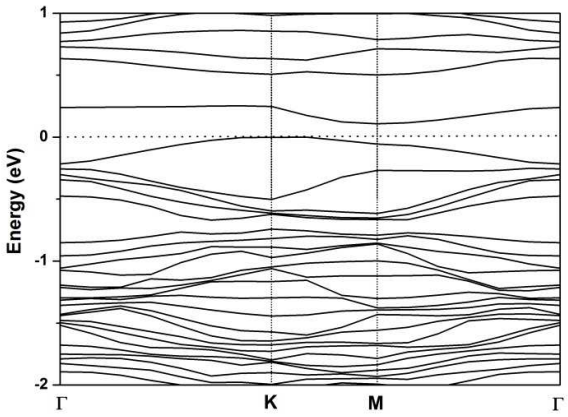

Figure 11. The band structure for HCHO adsorption on DV-Si with panel 2 configuration. The dash line indicates the Fermi level.

In the case of SW defected silicene sheet, the distortion of Si-Si bond opens up the band gap of 0.028 eV and does not affect the linear dispersion of the bands near the Fermi level E_F, which implies the possibility of still having a large Fermi velocity. Although, the presence of SW-defect changes the characteristics of the material, the

conductivity of the charge carriers will not be very different from the pristine case. For the system of HCHO adsorption, the band structure and the PDOS spectrum are depicted in Figure 12. The band gap of the HCHO/SW-Si system is distinctly expanded to the value of 0.190 eV and a new state near the Fermi level is introduced. With inspection of its PDOS, it can be seen that the states of O 2p strongly hybridize with Si 3p in the upper region of valence band, giving the main contribution of HCHO/SW-Si sheet interaction. In this process, the sheet donates electrons to the n_o' orbitals of HCHO and strengthens the interaction to make it a chemisorption. On the other hand, a small amount of empty orbitals at the bottom of conduction band indicates that some π^*_{CO} orbitals accept electrons and fall down into the region of valence band. This process weakens the intramolecular interaction between C and O. As a result, the C=O bond of HCHO is elongated to 1.452 Å, which is ~20% larger than that in free gas phase. The electronic donation of sheet and the downshift of the frontier orbitals of HCHO open up the band gap and make the sheet a semiconductor with a larger band gap than the sheet without HCHO adsorption. The changes originated from the HCHO adsorption make the sheet a promising candidate for the use of HCHO detecting.

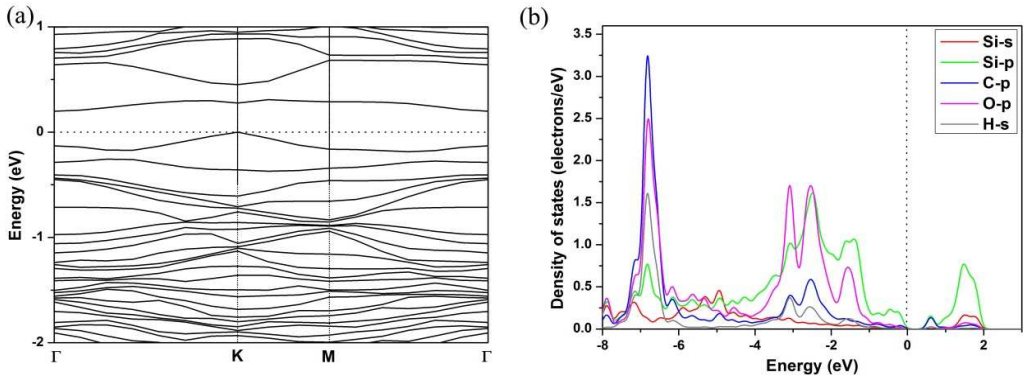

Figure 12. (a) The band structure and (b) PDOS for HCHO adsorption on SW defected silicene. The dash line indicates the Fermi level.

3.6 Effect of strain on formaldehyde adsorption on SW-Si sheet

As we all know, the external stress applied to graphene would affect the orbital hybridization of the carbon atoms and cause the formation of an extended π orbital with a localized electron (p_z orbital). As a result, the reactivity of graphene increases.[44] Motivated by this knowledge, we suspect that a nanomechanical modulation of strain may influence the chemical activity of SW defected silicene. Thus, we investigate the effects of strain applied to the SW defected silicene upon the adsorption of HCHO by varying the isotropic strain from 0% to 10% without any change on the crystal symmetries and honeycomb-like structures of the adsorbent. The in-plane tensile or compression strain is uniformly applied along lattice directions. The isotropic strain is defined as $\varepsilon = \Delta a/a_0$, where the lattice constants of the unstrained and strained supercell equal to a_0 and $a = \Delta a + a_0$, respectively. The stretching of SW-Si sheet is achieved by first elongating the optimized lattice constant from a_0 to a, and then the supercell was re-optimized. While undergoing strain, we

find the energy of SW-Si sheet increases with tensile strain (shown in Figure 13(a)), in agreement with previous reports of graphene under tensile strain. Si atom prefers to sp^3 hybridation in silicene which leads to a low-bulked sheet. When tensile strain increases, the bulkling of the sheet decreases which resulting in a destabilization of silicene. As a result, the total energy of the sheet increases. The variation of HCHO adsorption energies with lattice strain are shown in Figure 13(b). As the strain is increased, the adsorption energy of HCHO decreases. Under strain, the HCHO molecule is still chemisorbed on the SW-Si sheet with the same configuration of that binds with sheet without strain. Figure 14 is the PDOS of HCHO adsorption on SW-Si at ε=7%, in which the p orbital of O and C atoms hybridizing with the Si 3p orbital of SW-Si. The hybridization broadens and downshifts the Si 3p band. The obvious hybridization among the p-orbitals of Si and HCHO implies that the HCHO molecule is still chemisorbed to the defected silicene under tensile strain. It is also noted that at ε=10%, after HCHO adsorption, the defected silicene begins to have an obvious distortion in the defect area with Si-Si bond moves away from its original position.

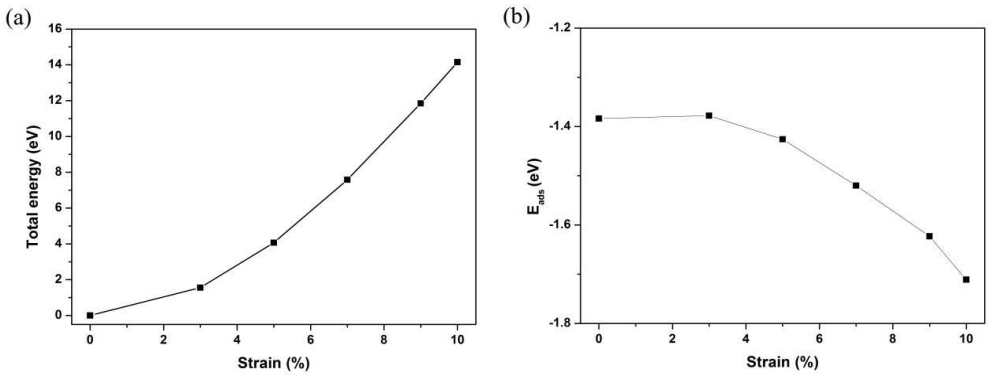

Figure 13. (a) Calculated total energy of silicene containing a SW defect and (b) HCHO adsorption energy E_{ads} on the SW-Si sheet as a function of lattice strain.

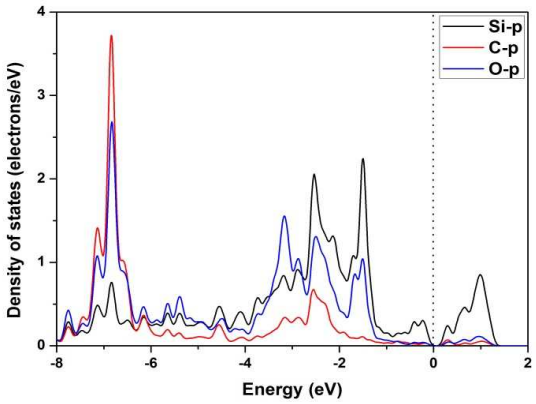

Figure 14. The PDOS of HCHO adsorption on SW-Si at ε=7%. The dash line indicates the Fermi level.

Figure 15 shows that the Si 3p-band center in SW-Si without the adsorption of HCHO molecule increases monotonically with tensile strain. Reduction in E_{ads} with tensile strain is due to the shift of the 3p-orbital energies of Si atom and the reduction in coordination. After HCHO adsorption, the Si 3p band center downshifts with strain as shown in Figure 15(b). The downshift of this 3p-band energy from the pristine state to the HCHO adsorption state is a measure of the relative relaxation of the system

energy upon HCHO adsorption. The shift becomes more negative for ε≤10%. The relative increase in the magnitude of this downshift for ε≤10% means that the system energy reduces by a larger amount upon HCHO chemisorption when strained, and thus, favors "stronger" chemisorption with lower E_{ads}, leading to increased reactivity. The same tendency also has been reported in the dissociative adsorption of hydrogen on silicene under strain.[24]

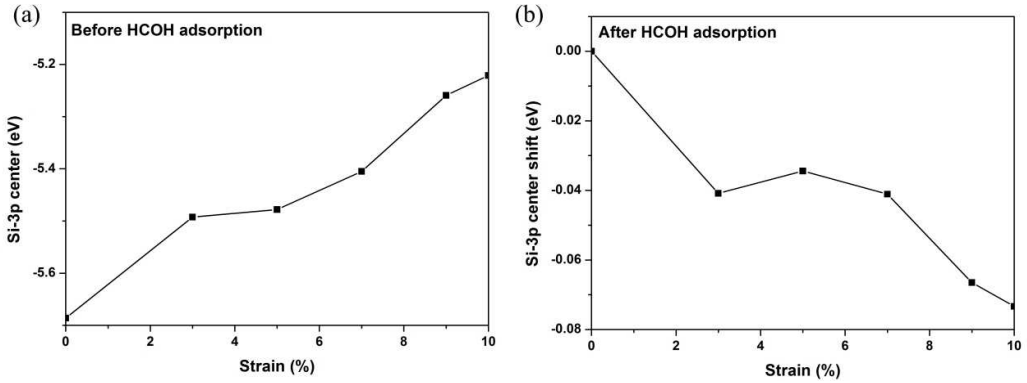

Figure 15. (a) The bonded Si 3p-band center before HCHO adsorption. (b) The shift of bonded Si 3p-band center from the pristine to the HCHO-adsorbed state, relative to the zero strain condition.

Furthermore, at ε=3%, 5% and 7%, the SW defected silicene still shows semiconductor characteristic with band gap of 0.163, 0.136 and 0.109, respectively (shown in Table 2). Although, SW defected silicene becomes metal when the strain increases to 9% and 10%, the electronic properties of SW defected silicene still shows apparent variation before and after HCHO adsorption under tensile strain 0-7%. This

indicates that even external stress exist in the adsorption system, SW-Si still shows the characters of gas sensor.

Table 2. Mulliken charge transfers from SW defected silicene under strain to HCHO molecule and band gap of SW defected silicene before (E_{gb}) and after HCHO adsorption (E_{ga}).

ε	Q (e)	E_{gb} (eV)	E_{ga} (eV)
3%	-0.418	0	0.163
5%	-0.411	0.028	0.136
7%	-0.409	0.028	0.109
9%	-0.408	metal	metal
10%	-0.412	metal	metal

4. Conclusions

To summarized, the adsorption of HCHO molecule on the pristine, Stone–Wales defected and double vacancy defected silicene were investigated by using the first-principles density functional theory. Detailed analysis of the geometrical structures and electronic properties of optimized configurations were performed. It is found that the adsorption of HCHO molecule on pristine silicene does not induce structural distortion in both molecule and silicene. Meanwhile, the molecule can be chemisorbed on SW defected and double vacancy silicene. Both defective silicene sheets exhibit large binding energy and short bond length. However, the electronic conductance changed obviously by the adsorption of HCHO molecule in SW-Si but not in DV-Si. Interestingly, chemical reactivity of SW-Si can be tuned by applying

external strain. The application of strain provides increases in the rate of reactivity, by a factor of up to10. It suggests that strain engineering of silicene provides a feasible way to modify the chemical activity of silicene.

Acknowledgements

The authors gratefully acknowledge financial support from NSFC (No. 21303054), China Postdoctoral Science Foundation (2013M540332) and the Fundamental Research Funds for the Central Universities under project No. 222201414040. All the computation simulation was undertaken with the resources provided from the High Performance Computing Center of East China University of Science and Technology.

Notes and references

1 A. K. Geim and K. S. Novoselov, *Nat. Mater.*, 2007, **6**, 183.

2 A. H. Castro Neto, F. Guinea, N. M. R. Peres, K. S. Novoselov and A. K. Geim, *Rev. Mod. Phys.*, 2009, **81**, 109.

3 K. S. Novoselov, A. K. Geim, S. V. Morozov, D. Jiang, Y. Zhang, S. V. Dubonos, I. V. Grigorieva and A. A. Firsov, *Science*, 2004, **306**, 666.

4 D. Jose and A. Datta, *Acc. Chem. Res.*, 2014, **47**, 593.

5 S. Cahangirov, M. Topsakal, E. Aktürk, H. Sahin and S. Ciraci, *Phys. Rev. Lett.*, 2009, **102**, 236804.

6 G. G. Guzmán-Verri and L. C. Lew Yan Voon, *Phys. Rev. B*, 2007, **76**, 075131.

7 T. Morishita, K. Nishio and M. Mikami, *Phys. Rev. B*, 2008, **77**, 081401.

8 J. F. Gao and J. J. Zhao, *Sci. Rep.*, 2012, **2**, 861.

9 P. D. Padova, C. Quaresima, C. Ottaviani, P. M. Sheverdyaeva, P. Moras, C. Carbone, D. Topwal, B. Olivieri, A. Kara, H. Oughaddou, B. Aufray and G. L. Lay, *Appl. Phys. Lett.*, 2010, **96**, 261905.

10 P. D. Padova, C. Quaresima, P. Perfetti, B. Olivieri, B. Leandri, B. Aufray, S. Vizzini and G. L. Lay, *Nano Lett.*, 2008, **8**, 271.

11 P. Vogt, P. D. Padova, C. Quaresima, J. Avila, E. Frantzeskakis, M. C. Asensio, A. Resta, B. Ealet and G. L. Lay, *Phys. Rev. Lett.*, 2012, **108**, 155501.

12 B. Feng, Z. Ding, S. Meng, Y. Yao, X. He, P. Cheng, L. Chen and K. Wu, *Nano Lett.*, 2012, **12**, 3507.

13 L. Meng, Y. Wang, L. Zhang, S. Du, R. Wu, L. Li, Y. Zhang, G. Li, H. Zhou, W. A. Hofer and H. J. Gao, *Nano Lett.*, 2013, **13**, 685.

14 J. W. Feng, Y. J. Liu, H. X. Wang, J. X. Zhao, Q. H. Cai and X. Z. Wang, *Comput. Mater. Sci.*, 2014, **87**, 218.

15 F. Banhart, J. Kotakoski and A. V. Krasheninnikov, *ACS Nano*, 2010, **5**, 26.

16. A.V. Krasheninnikov and K. Nordlund, *J. Appl. Phys.*, 2010, **107**, 071301.

17 C.X. Zhang, C. He, Z. Yu, L. Xue, K.W. Zhang, L.Z. Sun and J. Zhong, *Phys. Lett. A*, 2012, **376**, 1686.

18 H. Sahin, J. Sivec, S. Li, B. Paroens and F. M. Peeters, *Phys. Rev. B*, 2013. **88**, 045434.

19 J. F. Gao, J. F. Zhang, H. S. Liu, Q. F. Zhang and J. J. Zhao. *Nanoscale*, 2013, **5**, 9785.

20 S. Park, D. Srivastava and K. Cho, *Nano Lett.*, 2003, **3**, 1273.

21 M. A. Bissett, S. Konabe, S. Okada, M. Tsuji and H. Ago, *ACS Nano*, 2013, **7**, 10335.

22 5 O. Leenaerts, B. Partoens and F. M. Peeters, *Phys Rev B,* 2008, **77**, 125416.

23 T. O. Wehling, K. S. Novoselov, S. V. Morozov, E. E. Vdovin, M. I. Katsnelson, A. K. Geim and A. I. Lichtenstein, *Nano Lett.*, 2008, **8**, 173.

24 W. C. Wu, Z. M. Ao, C. H. Yang, S. Li, G. X. Wang, C. M. Li and S. Li, *J. Mater. Chem. C*, 2015, **3**, 2593.

25 V. J. Cogliano, Y. Grossem, R. A. Baan, K. Straif, M. B. Secretan and F. El Ghissassi, *Environ. Health Perspect*, 2005, **113**, 205.

26 M. Hauptmann, J. H. Lubin, P. A. Stewart, R. B. Hayes and A. Blair, *Am. J. Epidemiol.*, 2004, **15**, 1117.

27 B. Magada and H. El-Yazbi, *Anal. Lett.*, 1991, **24**, 857.

28 E. R. Kennedy and R. H. Hill, Jr. *Anal. Chem.*, 1982, **54**, 1739.

29 C. B. Xu, W. S. Yang, Q. Guo, D. X. Dai, T. K. Minton and X. M. Yang, *J. Phys. Chem. Lett.*, 2013, **4**, 2688.

30 J. Y. Kim, J. H. Lee, S. H. Hong and T. D. Chung, *Chem. Commun.*, 2011, **47**, 2892.

31 Q. X. Zhou, L. Yuan, X. Yang, Z. B. Fu, Y. J. Tang, C. Y. Wang and H. Zhang, *Chem. Phys.*, 2014. **440**, 80.

32 B. Delley, *J. Chem. Phys.*, 1990, **92**, 508.

33 B. Delley, *J. Chem. Phys.*, 1991, **94**, 7245.

34 B. Delley, *Int. J. Quantum Chem.*, 1998, **69**, 423.

35 J. P. Perdew, K. Burke and M. Ernzerhof, *Phys. Rev. B*, 1996, **77**, 3865.

36 H. J. Monkhorst and J. D. Pack, *Phys. Rev. B*, 1976, **13**, 5188.

37 S. Lebègue and O. Eriksson, *Phys. Rev. B*, 2009, **79**, 115409.

38 X. D. Li, J. T. Mullen, Z. H. Jin, K. M. Borysenko, M. B. Nardelli and W. K. Kim, *Phys. Rev. B*, 2013, **87**, 115418.

39 Y. C. Cheng, Z. Y. Zhu and U. Schwingenschlögl, *Europhys. Lett.*, 2011, **95**, 17005.

40 S. Cahangirov, M. Topsakal, E. Aktürk, H. Sahin and S. Ciraci, *Phys. Rev. Lett.*, 2009, **102**, 236804.

41 X. Peng and R. Ahuja, *Nano Lett.*, 2008, **8**, 4464.

42 L. J. Zhou, Z. F. Hou and L. M. Wu, *J. Phys. Chem. C*, 2012, **116**, 21780.

43 X. Qin, Q. Y. Meng and W. Zhao, *Surf. Sci.,* 2011, **605**, 930.

44 V. J. Surya, K. Iyakutti, H. Mizuseki and Y. Kawazoe, *Comput. Mater. Sci.*, 2012, **65**, 144.